Proceedings of DETC2000
2000 ASME Design Engineering Technical Conference
September 10 - 13, 2000, Baltimore, Maryland

DETC2000/MECH-14145

PARTIALLY CONSTRAINED COMPLIANT STAGES FOR HIGH RESOLUTION IMPRINT LITHOGRAPHY

B. J. Choi, S. Johnson[1] and S.V. Sreenivasan[2]
Dept. of Mechanical Engineering

M. Colburn, T. Bailey and C.G. Willson
Dept. of Chemical Engineering
University of Texas at Austin
Austin, Texas 78712

ABSTRACT

This paper presents design of partially constrained compliant stages for high-resolution (sub 100*nm*) imprint lithography machines. The kinematic designs of the stages allow passive alignment of two flat surfaces and enable shear-free separation. This stage is a critical component in a new lithography process known as Step and Flash Imprint Lithography (SFIL). The orientation stage requirements are distinct from those used in traditional photolithography since the depth of focus of projection optics allows for larger errors in the alignment process. Experiments have been performed to demonstrate sub 100*nm* imprints on silicon substrates.

1 INTRODUCTION

Step & Flash Imprint Lithography (SFIL) is a high throughput novel approach that can potentially generate circuit patterns with sub 100*nm* line width (Colburn, 1999). SFIL uses no projection optics and operates at room temperature and low pressure between the template and substrate surfaces. The process largely relies on chemical and mechanical processes to transfer patterns. One could probably best describe SFIL as a micro-molding process (See (Chou, 1996; Haisma, 1996; Wang, 1997; Widden, 1996; and Xia, 1998) for other imprint processes under development). SFIL and other imprint lithography techniques are similar in the fact that they use the topography of a template to define the pattern created on the substrate. The key difference between SFIL and other imprint lithography techniques is the use of a liquid etch barrier. This low viscosity solution eliminates the need for high temperatures and pressures. High temperatures and pressure can cause major technical problems in accurate overlaying of multiple layers of a device and is hence undesirable.

1.1 Challenges to Optical microlithography

Figure 1.1 illustrates the typical industrial optical microlithography process. A quartz photomask defines the master circuit image to be transferred to the wafer. The circuit pattern is written into a thin layer of chromium on the photomask using direct write electron beam lithography. This layer of chromium blocks light shining on the photomask. When a light source illuminates the photomask, the pattern written in the chromium is projected onto a wafer below.

The imaging layer of a photoresist polymer captures the aerial image projected onto the wafer. Light alters the chemical structure of the photoresist and changes its solubility. Rinsing the wafer in a developer solution selectively dissolves the photoresist leaving a layer of photoresist in the shape of the circuit pattern.

Once the imaging layer has been patterned, an etch process transfers the circuit image to the transfer layer. The remaining imaging layer is then stripped from the wafer. At this point, the transfer layer is patterned in the shape of the circuit image on the photomask. The transfer layer then serves as a mask for subsequent manufacturing steps such as etching, metal deposition, epitaxial growth, and ion implantation.

---

[1] Currently with 3M, Austin, TX.
[2] Corresponding author: Tel.: 512-471-6546: fax: 512-471-8727.
E-mail address: sv.sreeni@mail.utexas.edu.

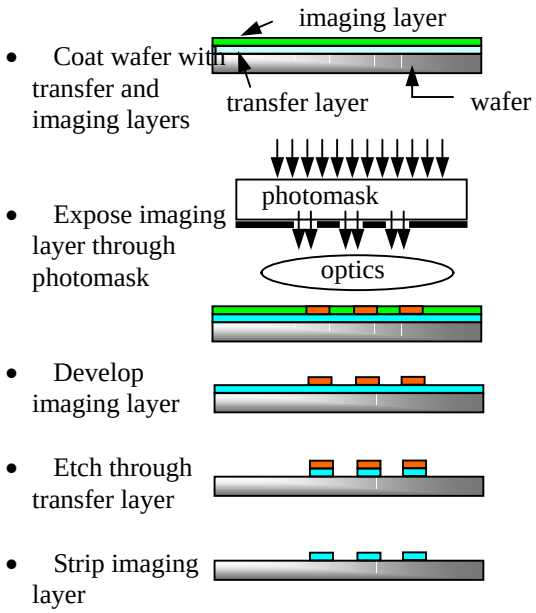

Figure 1.1 Optical microlithography process

Because today's optical lithography machines are diffraction limited, much of the technological investment goes into optical projection systems. Higher resolution imaging can be obtained by increasing the size of lens, or by decreasing the wavelength of light used. Large lenses are more difficult to manufacture and, thus, more expensive. It is not uncommon for lens systems in today's optical lithography machines to weigh hundreds of pounds and cost several million dollars.

Investments in reducing the wavelength of light used to print images have reduced minimum printable line widths. Many of today's steppers use 248 *nm* Deep Ultra Violet (DUV) light and 193 *nm* and 157 *nm* systems are in development and will decrease minimum printable line widths. 15 *nm* Extreme Ultra Violet (EUV) and X-ray lithography technologies offer potential for decreasing line widths to even smaller dimensions, but these techniques present significant technical challenges and prohibitive cost. Materials that are transparent to DUV light are opaque in the EUV and X-ray regions, so these new technologies may only use reflective optics. Furthermore, EUV and X-ray sources with sufficient intensity to print images are rare and expensive. The technical challenge and cost of implementing EUV and X-ray lithography technologies clearly warrant the investigation of other pattern transfer technologies for use in the semiconductor and micro-machining areas.

1.2 Challenges to Step and Flash Imprint Lithography

Figure 1.2 illustrates SFIL process and Figure 1.3 shows subsystems include sensing, stage actuation, light source, etc. An important aspect of the research deals with the design of a machine to implement the SFIL process. Such a machine must

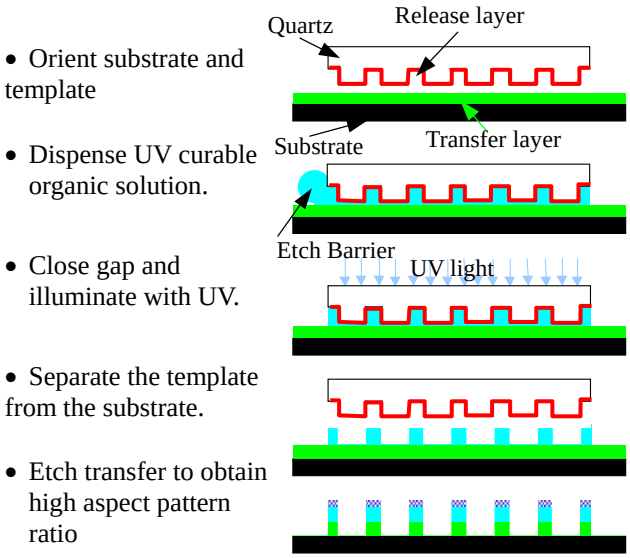

Figure 1.2 SFIL Process

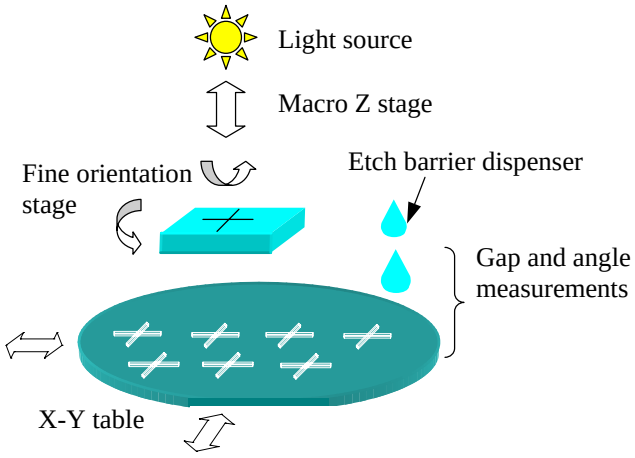

Figure 1.3 SFIL subsystems

hold a template and a substrate. It must bring them into near contact, dispense etch barrier solution, and irradiate this sandwich structure with ultraviolet light. One focal point of this machine development deals with the interaction of the template and substrate. The template and substrate must be in near-uniform contact when irradiated with UV light. Finally, when the template and substrate are separated, shearing at the interface should be avoided since it will destroy the imprinted pattern. It is not sufficient to make the template parallel to the wafer. The gap has to be controlled to as low a level as possible to avoid undesirable "base layer" (see Fig 1.4 (b) and (c))

Other important research issues related to SFIL are in the synthesis of appropriate materials with tailored surface and curing characteristics. These issues are discussed elsewhere (Colburn, 1999).

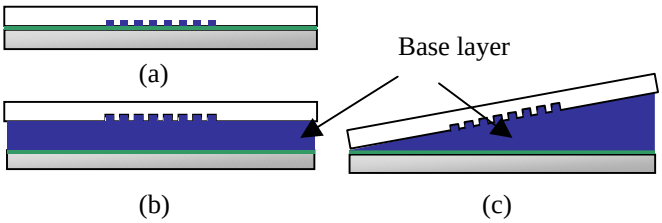

Figure 1.4 (a) Ideal alignment, (b) thick base layer, and (c) wedged base layer

2 PARTIALLY CONSTRAINED ALIGNMENT STAGES

In this section, kinematics of alignment stages for the SFIL is presented. The alignment stage is a critical component of the imprint lithography machine as it provides fine motion control at the template-substrate interface. In Section 2.1, alignment kinematics between two flat surfaces are discussed. Alignment is necessary to compensate for errors from several sources such as machining, machine assembling, and positioning uncertainty involved in wafer and template loading/unloading. In Section 2.2, a kinematic design of a partially constrained ideal stage is introduced. In Section 2.3, this ideal kinematic stage is used as a starting point to develop a distributed flexure-based stage. In Section 2.4, a template stage with remote compliance axes is introduced for a multi imprint machine.

2.1 Kinematics between two flat surfaces

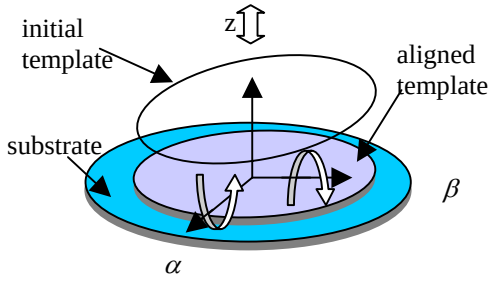

Figure 2.1 Two flats representing template and wafer

Figure 2.1 shows two flat surfaces representing a template and substrate respectively. As described earlier, proper alignment between these two flats ideally leads to a perfectly uniform surface contact between them. Such an alignment can be accomplished with one translation motion (z displacement) and two tilting motions (α and β) between two flats. These relative motions can be implemented by either fixing the template and mounting the substrate on a three degree-of-freedom (DOF) stage or vice-versa. If a course pre-calibration ($5–10\mu m$ range) is performed between the template and the wafer chuck every time a new template is installed, then the desired maximal relative displacements of the stage are of the order of 10microns, and the desired maximal tilting motions are of the order of 1mrads.

Based on the discussion above we need partially constrained stages for imprinting flats surfaces. The motion of these stages can be generated either by passive compliance or by active actuation. Tilting motions at a passive stage is generated by z-direction force between two flats. Passive compliance is easy to implement and does not require sophisticated alignment error sensing and control. Therefore, this option has been pursued here. However, active stages have important advantages that make it necessary to study them. Some of the discussion in the following sections may also apply to active stages. Experimental investigation has only been done using passive stages. Ongoing research includes the development of active stages.

2.2 Ideal kinematic stages

As described in the previous section, template-substrate sets can be aligned using three DOF stages. Here, a kinematic design of ideal alignment stages is presented. Ideal stages are assumed to be composed of perfect rigid bodies and joints. Non-ideal behavior including distributed structural compliance, backlash and stiction in joints, etc. are neglected. Ideal kinematic stages provide insight into the geometry and force transmission at the template-substrate interface. This insight is then extended to the design of distributed flexure stages with selectively compliant directions. (Section 2.3).

A design of a three DOF stage is shown in Figure 2.2 (a) in its nominal state. This stage has a parallel kinematic structure and it was chosen since parallel mechanisms are known to possess higher stiffness and accuracy (Lee, 1988; Waldron, 1989). The connection from the base platform to the moving platform is via a combination of a revolute (R) joint, a prismatic (P) joint and a ball (B) joint (a combination of these three joints is referred to as 'leg i', Figure 2.2 (b)). The reference frame at the moving platform is defined as x_1-y_1-z_1. For the base platform, the reference frame is defined as x_0-y_0-z_0. The location of ball joint 'i' is defined as $\mathbf{p}_i$.

Kinematic design of these stages is studied using screw system theory (Roth, 1984; Hunt, 1990). Screw system theory

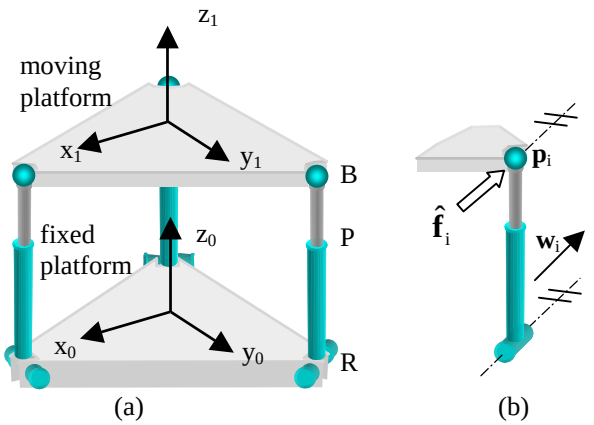

Figure 2.2 (a) Three-degree-of-freedom in-parallel mechanism, (b) Leg "i"

provides a unified geometric approach to the study of spatial (6-dimensional) motion and force systems of mechanisms.

An instantaneous screw axis ($: a unit screw), is a purely geometric quantity that represents a line in space along with a pitch, *h*. It can be expressed as a 6 by 1 vector as follows:

$$\$= \begin{pmatrix} \mathbf{w} \\ \boldsymbol{\rho} \times \mathbf{w} + h\mathbf{w} \end{pmatrix} \qquad (2.1)$$

where, $\mathbf{w}$ is a unit vector parallel to the line and $\boldsymbol{\rho}$ is the position vector of any point on the line. In the case of an infinite pitch, $\$ = [\mathbf{0}^T; \mathbf{w}^T]^T$. The velocity state of a rigid body, its motor $\hat{\mathbf{v}}$ and the force system on a rigid body, its wrench $\hat{\mathbf{f}}$, can be written in terms of screws as:

$$\hat{\mathbf{v}} = \omega \$_v, \qquad \hat{\mathbf{f}} = f\,\$_f, \qquad (2.2)$$

where, ω is the angular velocity about the screw $\$_v$ and f is a pure force acting along the screw $\$_f$.

When the wrench applied to a rigid body does no work on the motor of that body, then the wrench is said to be reciprocal to the motor. The two screws corresponding to the wrench and the motor satisfy the following purely geometric condition:

$$(\$_v)^T\, \boldsymbol{\Pi}\, \$_f = 0, \qquad (2.3)$$

where, $\boldsymbol{\Pi} = \begin{bmatrix} 0_3 & \mathbf{I}_3 \\ \mathbf{I}_3 & 0_3 \end{bmatrix}$, I3 is a 3 by 3 identity matrix.

Now, it is shown that the motion capability if the stage of Figure 2.2 (a) is the same as the one required for aligning two flats. Using the reciprocity between motor and wrench systems [Ro84], the motion capability of the moving platform is explored. As shown in Figure 2.2 (b), when a zero pitch wrench (pure force), $\hat{\mathbf{f}}_i$, is applied at the center of the ball joint, $\mathbf{p}_i=(p_{xi}, p_{yi}, p_{zi})^T$, parallel to the axis of the revolute joint, $\mathbf{w}_i=(w_{xi}, w_{yi}, w_{zi})^T$, this wrench does not cause any displacement in the joints. Using the x_1-y_1-z_1 reference frame, three wrenches that are reciprocal to these legs are represented as,

$$^1\hat{\mathbf{f}}_i = f_i\,(^1w_{xi}, {}^1w_{yi}, 0; 0, 0, {}^1w_{xi}\,{}^1p_{yi} - {}^1w_{yi}\,{}^1p_{xi})^T, \quad i = 1, 2 \text{ and } 3, \qquad (2.4)$$

where, the first three components are the direction cosines of the revolute joint axis and the second three components are the cross product of $\mathbf{p}_i$ with the direction cosine components. Here, a pre-superscript, '1', represents components defined in x_1-y_1-z_1 frame.

The wrench space (R) of these three reciprocal forces can be spanned by $(\mathbf{i}; \mathbf{0})^T$, $(\mathbf{j}; \mathbf{0})^T$ and $(\mathbf{0}; \mathbf{k})^T$, where $\mathbf{i} = (1\ 0\ 0)^T$, $\mathbf{j} = (0\ 1\ 0)^T$, $\mathbf{k} = (0\ 0\ 1)^T$ and $\mathbf{0} = (0\ 0\ 0)^T$. The motion capability of the moving platform can be obtained as a linear combination of these basic screws each of which is reciprocal to R and they can be computed using condition of Eqn. (2.3). It is well known that when the rank of R is *m*, the rank of the corresponding motion space is given by 6-*m*. Therefore, the moving platform possesses three DOF and the motion space is spanned by $(\mathbf{i}; \mathbf{0})^T$, $(\mathbf{j}; \mathbf{0})^T$ and $(\mathbf{0}; \mathbf{k})^T$. This is a special situation where the symmetry of the mechanism leads to the screws of the reciprocal wrench space and the motion space being identical.

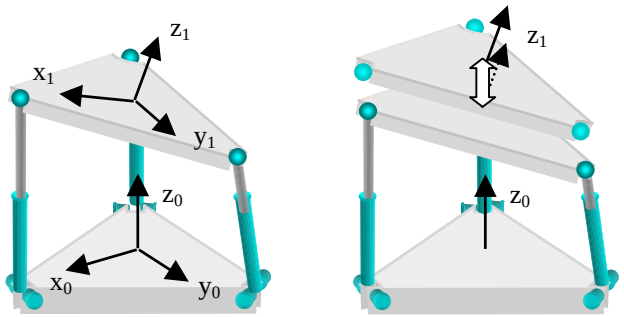

(a) (b)

Figure 2.3 (a) Three-degree-of-freedom in-parallel mechanism in an off-nominal configuration; (b) pure translation motion of moving platform in the vertical direction with respect to base platform

The first two motion screws represent two tilting motions whose axes lie on the moving platform, and the third motion screw represents a pure translation orthogonal to the moving platform. Therefore, as described in Section 2.1.1, this three DOF stage can be used for the alignment of two flats.

Due to various geometric errors, the R-P-B stage will in general not be used exactly in its nominal position of Figure 2.2 (a). In non-nominal positions (shown in Figure 2.3 (a)), a weak coupling is present between the alignment motion directions and the undesirable motion directions. The effects of this coupling on the imprint process are now investigated. In x_0-y_0-z_0 frame, the three reciprocal wrenches are represented as

$$^0\hat{\mathbf{f}}_i = f_i\,(^0w_{xi}\ {}^0w_{yi}\ 0; {}^0\mathbf{w}_I \times {}^0\mathbf{p}_i)^T, \ i = 1, 2, 3. \qquad (2.5)$$

Using reciprocity and Eqn. (2.3), we can find one infinite pitch motion of the moving platform; $(\mathbf{0}; \mathbf{k})^T$. This infinite pitch motor represents the translation of the moving platform in the vertical direction with respect to the base platform (see Figure 2.3 (b) for the translation).

Two other motions are available as a basis of the null space of a 4 by 6 matrix; $[\boldsymbol{\Pi}^0\hat{\mathbf{f}}_1, \boldsymbol{\Pi}^0\hat{\mathbf{f}}_2, \boldsymbol{\Pi}^0\hat{\mathbf{f}}_3, (\mathbf{0}; \mathbf{k})^T]^T$. These two motions are not pure tilting motions, but coupled with undesirable translation motions. Therefore, a non-nominal mechanism leads to a translation which is not exactly along z_1. In addition, tilting motions can cause undesirable motions along x_1 and y_1.

2.3 Flexure-based alignment stages

The ideal kinematic stage of Section 2.2 has several practical limitations with respect to high-resolution lithography. Presence of sliding contacts in joints can cause wear, generate undesirable particles and lead to stiction that makes precision motion control difficult. Particles on the template and substrate generate major defects in the SFIL process. Presence of clearances in joints can lead to reduced repeatability in the motion of the mechanism.

Flexures generate motion by elastic deformation and can avoid all the problems associated with joints. Also, provided elastic and fatigue limits are not exceeded, flexures can provide

extremely repeatable motion and long life for the stage. Flexure stages are becoming quite common in the precision engineering industry (Smith, 1992).

A major challenge associated with the use of flexures is the design of mechanisms with prescribed motion-force characteristics. Here, a procedure is described to obtain a conceptual design of a flexure mechanism whose motion capability is similar to that of the ideal stage of Section 2.2. Next, a screw theory based analysis scheme is presented to obtain the principal motion capability of this stage to ensure that it is similar to the ideal stage.

The basic element of the flexure is derived from the work presented in Badami, et al. (1996). They presented a ring that is comprised of three fixed-fixed beams. The mid-point of each of these beams provide a vertical deflection due to an applied vertical load. This vertical spring can be considered to be equivalent to a leg of the R-P-B stage where the P joint is a passive linear spring. A modified version of this design yields the distributed flexure stage of Figure 2.4.

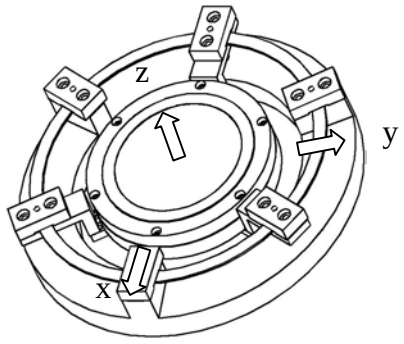

Figure 2.4 Distributed flexure design

The three mid-points of the fixed-fixed beams are connected to the vacuum chuck that holds the wafer. The parameters of the ring (material and geometry) can be arrived at by using the desired motion range for the z-translation and the two tilting motions

This distributed flexure stage poses an interesting analysis problem: What is the best way to determine the principal motion capabilities of a mechanism incorporating distributed compliance? Following sections present an analysis that looks at a generalized compliance matrix. A finite element model is used to compute the non-ideal compliance matrix of the distributed flexure stage. The results of the finite element model are then used to examine the stage's principal motion capabilities.

2.3.1 Basis of comparison

Griffis and Duffy (1991) and Patterson and Lipkin (1993) present a format for investigating the motion capabilities of compliant structures. A rigid body fully supported by an elastic system has six DOF. The motion capabilities of the rigid body may be determined by examining the elastic structure supporting the body. For example, the motion capability of the vacuum chuck in the distributed flexure stage may be determined by examining the compliant structure of the aluminum flexure ring. Similarly, the motion capability of the top plate of the R-P-B stage with passive spring along the P joint may be determined by examining the structure supporting the plate.

Screw theory offers a means of quantifying the motion capability of a compliant structure. A wrench, $\hat{\mathbf{f}}$, and twist, $\hat{\mathbf{T}}$, may be used to describe the motion of a rigid body supported by a compliant structure. A wrench in ray coordinates, $\hat{\mathbf{f}}=[\mathbf{f}^T\ \boldsymbol{\tau}^T]^T$, consists of a force ($\mathbf{f}$) along and a moment ($\boldsymbol{\tau}$) about a screw axis. A twist in axis coordinates, $\hat{\mathbf{T}}=[\underline{\boldsymbol{\delta}}^T\ \underline{\boldsymbol{\gamma}}^T]^T$ represents a small displacement about a screw axis. $\underline{\boldsymbol{\delta}}$ represents a linear deflection along and $\underline{\boldsymbol{\gamma}}$ represents a rotational deflection about a screw axis. A compliance matrix $\mathbf{C}$ relates a wrench to a twist:

$$\hat{\mathbf{T}} = \mathbf{C}\hat{\mathbf{f}} \qquad (2.6)$$

The $\boldsymbol{\Pi}$ operator may be used to convert a twist in axis coordinates, $\hat{\mathbf{T}}$, to a twist in ray coordinates, $\hat{\mathbf{t}}$:

$$\hat{\mathbf{t}} = \boldsymbol{\Pi}\,\mathbf{C}\,\hat{\mathbf{f}} \qquad (2.7)$$

By assuming that the wrench $\hat{\mathbf{f}}$ and twist $\hat{\mathbf{t}}$ are scalar multiples of the same screw, it is possible to construct an eigenvalue problem:

$$\lambda\,\mathbf{e} = \boldsymbol{\Pi}\,\mathbf{C}\,\mathbf{e} \qquad (2.8)$$

This formulation yields six eigenvalues λ_i and six eigenvectors or eigenscrews $\mathbf{e}_i$. λ_i represents the ratio of angular deformation to force. Note that Eqn. 2.8 solves the eigenvalue problem for the matrix $\boldsymbol{\Pi}\mathbf{C}$. The eigenvalues of $\mathbf{C}$ are frame dependent and the resulting eigenvectors do not provide physically meaningful quantities of the motion capabilities of the mechanism.

These eigenscrews of $\boldsymbol{\Pi}\mathbf{C}$ represent the fundamental modes of a compliant mechanism. All of the motions of a compliant mechanism may be modeled as linear combinations of the fundamental eigenscrews.

Eigenscrews with zero eigenvalues can be examined to gain insight into the motion capability of a partially constrained mechanism. The space spanned by all eigenscrews with zero eigenvalues is equal to the space spanned by all wrenches reciprocal to the mechanism.

2.3.2 R-P-B stage compliance

The derivation of the stage's compliance matrix begins with an examination of the six screws that span the space of all possible wrenches of the mechanism. Figure 2.5 illustrates these screws. $\$_1$, $\$_2$, and $\$_3$ represent the wrenches along the legs. $\$_1^r$, $\$_2^r$, and $\$_3^r$ represent the screws reciprocal to the system. A wrench applied along these screws will be transmitted through the linkage and cause no movement.

These six screws can be assembled into an operator that maps a general wrench applied to the system into reciprocal and non-reciprocal components. This operator is **J**:

$$\mathbf{J} = [\,\$_1 \;\; \$_2 \;\; \$_3 \;\; \$_1^r \;\; \$_2^r \;\; \$_3^r\,] \qquad (2.9)$$

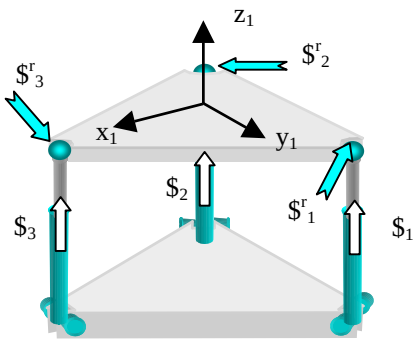

Figure 2.5 Screw representation of R-P-B stage

It can be shown (Johnson, 1999) that the compliance matrix **C** of the passive R-P-B stage is given by $\mathbf{C} = \mathbf{J}^{-T}\boldsymbol{\Delta}\mathbf{J}^{-1}$ and $\boldsymbol{\Pi}\mathbf{C}\,\hat{\mathbf{f}} = \hat{\mathbf{t}}$, where,

$$\boldsymbol{\Delta} = \begin{pmatrix} c_1 & 0 & 0 & 0 & 0 & 0 \\ 0 & c_2 & 0 & 0 & 0 & 0 \\ 0 & 0 & c_3 & 0 & 0 & 0 \\ 0 & 0 & 0 & 0 & 0 & 0 \\ 0 & 0 & 0 & 0 & 0 & 0 \\ 0 & 0 & 0 & 0 & 0 & 0 \end{pmatrix}, \qquad (2.10)$$

and c_i is the compliance of the linear spring of leg 'i'. Note that the compliance of the reciprocal springs is represented with a value of zero to denote infinite stiffness in the reciprocal directions.

The eigenscrews and corresponding eigenvalues for the R-P-B stage follow directly from the matrix $\boldsymbol{\Pi}\mathbf{C}$. The eigenstructure problem has been solved for typical parameters of the stage. Matrices **V** and **D** present the eigenscrews and eigenvalues of the matrix $\boldsymbol{\Pi}\mathbf{C}$. Each column of **V** corresponds to one eigenscrew of $\boldsymbol{\Pi}\mathbf{C}$. Each diagonal element of **D** gives the eigenvalue for the corresponding eigenscrew in **V**.

$$\mathbf{V} = \begin{pmatrix} 1 & 0 & 0 & 0 & -1 & 0 \\ 0 & 1 & 0 & 0 & 0 & -1 \\ 0 & 0 & 0 & 0 & 0 & 0 \\ 0 & 0 & 0 & 0 & 0 & 0 \\ 0 & 0 & 0 & 0 & 0 & 0 \\ 0 & 0 & 1 & -1 & 0 & 0 \end{pmatrix}, \text{and}$$

$$\mathbf{D} = \begin{pmatrix} 0 & 0 & 0 & 0 & 0 & 0 \\ 0 & 0 & 0 & 0 & 0 & 0 \\ 0 & 0 & 0 & 0 & 0 & 0 \\ 0 & 0 & 0 & 0 & 0 & 0 \\ 0 & 0 & 0 & 0 & 0 & 0 \\ 0 & 0 & 0 & 0 & 0 & 0 \end{pmatrix}.$$

All the eigenvalues of $\boldsymbol{\Pi}\mathbf{C}$ (diagonal elements of **D**) are zero. This indicates that all of the eigenscrews (columns of **V**) lie in the reciprocal wrench space $\$_f$ of the mechanism. In fact the eigenvector space is defective since they only span a 3 space. It has been observed in this research that partially constrained compliant system can lead to defective eigenvector spaces. It is well-known in the linear algebra literature that repeated eigenvalues are a pre-requisite for a defective eigenvector space. The eigenvalues of non-ideal stages that have very similar but not identical compliance characteristics as an ideal stage are not likely to be exactly zero. This leads to a case where a near defective matrix possesses six linearly independent eigenvectors. As shown in the following analysis, this leads to problems in using the eigenstructure as a means to effectively compare ideal R-P-B and flexure stages.

A deficient eigenvector space by itself does not create a problem. Difficulties arise, however, if attempts are made to solve the eigenvalue problem for the compliance matrix of a near-ideal stage that has been numerically derived. The finite element model derivation of the distributed flexure stage's compliance matrix is such a case. A flexure stage's compliance matrix is both numerically derived and has a near-deficient eigenvector space. Solving for the eigenvalues and eigenvectors of $\boldsymbol{\Pi}\mathbf{C}$ for the distributed flexure stage yields a set of distinct eigenvalues (that are approximately zeros) and spurious eigenvectors that span the six space. These eigenvectors cannot be interpreted to gain insight into the physical system's motion capability (Johnson, 1999).

While the eigenstructure of a compliant mechanism is a good indicator of its kinematic and load bearing characteristics, its use in comparing the ideal R-P-B stage and the flexure stage is limited. The repeated zero eigenvalues and a defective eigenvector space of the ideal stage lead to poorly conditioned numerical approximations of the flexure stage. A robust numerical scheme is therefore required for comparing the ideal and flexure stages. The following section presents such an approach based on strain energy.

2.3.3 The use of strain energy as a metric

The difficulty of characterizing the behavior of numerically computed non-ideal compliant structures using eigenvalues and eigenvectors illustrates the need for an alternative metric to analyze the motion capabilities of compliant spatial mechanisms. The physical quantity of strain energy may be used as such a metric. The amount of work done by a force is the product of a force and the distance through which it acts:

$$W = F\,d \qquad (2.11)$$

where, W is a work done by a force F (units of energy), F is an applied force (units of force), and d is the distance through which the force acts (units of length) The work done by a wrench acting on a compliant structure may be calculated in a similar manner:

$$W = \hat{\mathbf{f}}^T\,\boldsymbol{\Pi}\,\hat{\mathbf{t}} = \hat{\mathbf{f}}^T\,\mathbf{C}\,\hat{\mathbf{f}} = E \qquad (2.12)$$

where, $\hat{\mathbf{f}}$ is a wrench applied to the structure (units of force, torque), $\hat{\mathbf{t}}$ is a twist representation of structure's deflection (units of length, rotation), and E is strain energy stored in the deformed compliant structure (units of energy). Wrenches of the same magnitude applied along stiff portions of an elastic structure will cause little deformation and store little strain energy in the system.

This relationship can be exploited to find wrenches that are "near-reciprocal" to a mechanism. Given an applied wrench and resulting twist, one can calculate the strain energy stored in a compliant structure via Eqn. (2.12). Wrenches that generate little or no strain energy in the structure are assumed to be near-reciprocal wrenches.

The first step in determining the motion capability of the distributed flexure stage using the concept of strain energy is to compute the stage's compliance matrix. Traditional methods of computing compliance matrices, such as the one used to determine the compliance matrix of the ideal stage, rely on the geometry of a mechanism and the location of all of its joints. The lack of well-defined joints in the distributed flexure stage makes it difficult to apply these methods.

A finite element model provides an alternative means of generating a structure's compliance matrix. Finite element codes allow the user to compute the deflection of a compliant mechanism for a given load. If one knows the deflection of a compliant mechanism for six linearly independent wrenches, one can compute the mechanism's compliance matrix:

$$\mathbf{\Pi C F} = \mathbf{T} \qquad (2.13)$$

$$\mathbf{\Pi C} = \mathbf{T}\,\mathbf{F}^{-1} \qquad (2.14)$$

where, $\mathbf{F}$ = 6 by 6 matrix of six applied wrenches $\hat{\mathbf{f}}_i$

$\mathbf{T}$ = 6 by 6 matrix of corresponding twists $\hat{\mathbf{t}}_i$

$\mathbf{C}$ = 6 by 6 compliance matrix

Boundary conditions are defined to allow no linear or rotational displacement at the three locations where the flexure ring connects to the base. These conditions simulate a rigid structure supporting the flexure ring. Six linearly independent wrenches were applied to the structure. Each column of matrix $\mathbf{F}$ represents a wrench applied to the FEA model.

The finite element model computes a deflection for every individual applied wrench. Figure 2.6 illustrates the finite element model computation of the stage's deflection under a vertical load. Shading indicates von Mises stresses in the structure as it deforms.

The finite element model outputs the deflection of the stage as a set of node deflections. Waldron (1993) outlines a method for relating initial and final locations of three points on a rigid body that undergoes a displacement to an equivalent screw displacement based on Chasle's theorem. This method was used to convert the nodal displacements of three points on the vacuum chuck to a corresponding screw displacement. By assuming small displacements, these screws were represented as twist vectors. Each column $\mathbf{T}$ represents the twist due to the wrench represented by the corresponding column of $\mathbf{F}$. $\mathbf{F}$ represents forces in Newtons and moments in Newton-millimeters (N-mm). $\mathbf{T}$ represents rotations in radians and translations in millimeters.

$$\mathbf{T}=\begin{pmatrix} -0.0005 & 0 & 0 & 0 & -0.00116 & 0.0023 \\ 0 & 0.0016 & 0.0005 & 0 & 0.0007 & 0.0101 \\ 0 & 0 & 0 & -0.0001 & 0 & 0 \\ 0 & 0.0024 & 0.0197 & 0 & 0.0013 & 0.0206 \\ 0.0198 & 0 & 0 & -0.0005 & 0.0225 & -0.0045 \\ 0.0001 & -1.4128 & -0.0013 & 0 & 0.0011 & -0.0369 \end{pmatrix}$$

Using the computed compliance matrix and the strain energy equation (Eqn. (2.12)) for applied wrenches, wrenches that provide very low strain energy are sought and identified as near-reciprocal wrenches. Table 2.1 lists strain energies calculated from wrenches and twists taken from the FEA model of the flexure stage.

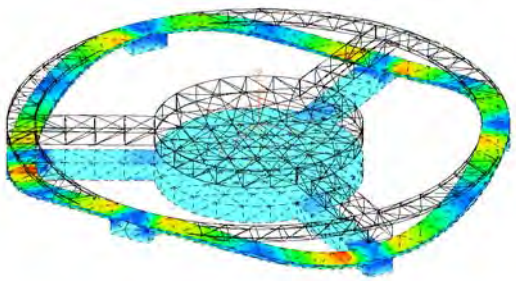

Figure 2.6 Deflected finite element model

Strain Energy	Applied wrench
1.3125	15 lb. force along x axis
1.3185	15 lb. force along y axis
94.6136	15 lb. force along z axis
119.0054	10 in-lb. torque about x
116.1306	10 in-lb. torque about y
1.4617	10 in-lb. torque about z

Table 2.1 Strain energy in flexure stage

Small strain energies indicate that wrenches consisting of forces along the x and y axes and moments about the z axis are near-reciprocal to the distributed flexure stage. These three wrenches span the space of wrenches reciprocal to the stage. Wrenches with large strain energies are not reciprocal to the stage. These results confirm that the distributed flexure stage exhibits the motions that are desired in a wafer alignment stage and are similar to the R-P-B stage. The flexure stage allows rotations about x and y and translation in z. At the same time, it has low translation in x and y and rotation about z. For a given magnitude of force (moment), the strain energy (or deflections) in the reciprocal directions are two orders of magnitude lower as seen from Table 2.1. Further, since forces imparted to the wafer (moving platform of the stage) is largely vertical, the ratio of the force along the wafer surface to the force orthogonal to the wafer is tan δ, where δ is a small angle (conservative bound = 1°). Therefore, the deflection of the stage along the vertical (z) direction is several orders of

magnitude higher than that along x and y ($1\mu m$ deflection in z leads to less than $1nm$ deflection along x and y). Similarly, tilting deflections along x and y is 4 orders of magnitude higher than tilting about z. Therefore, the flexure stage exhibits shear-free motion characteristics appropriate for use as an imprint lithography alignment stage.

2.4 Template Orientation Stage for Multi-Imprint Machine

In semiconductor manufacturing, multiple devices are patterned onto a single substrate by moving a wafer to various positions while holding a mask or a template stationary in x and y directions. A discussion of orientation alignment stages for multi-imprint machines is now provided. For the single imprint machine (Figure 3.1), a compliant stage that holds a wafer chuck was designed.

In order to eliminate relative lateral motions between the template and wafer, the compliance axes of the passive stage have to lie on the template-wafer interference. However, for multi-imprint processes, it has been noticed that the passive wafer stage cannot perform proper orientation motions when the template is not at the center of a wafer (see Figure 2.7). Hence a new orientation stage design that can tilt the template instead of the wafer is desired. Since, for a practical template stage, all mechanical components of the orientation stage should be positioned further from the wafer surface than the template surface, a template orientation stage that can tilt the template about "remote axes" was developed.

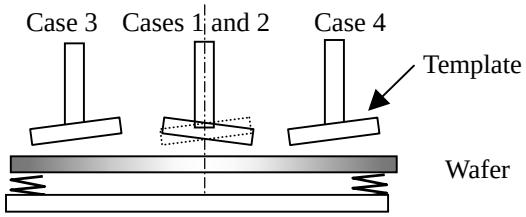

Figure 2.7 Possible configurations of templates and compliant wafer stage (a wafer stage works for Cases 1, 2, and 3 only)

Figure 2.8 shows a simple four-bar-linkage with ideal links and joints in its normal and rotated configurations. The angle between the line passing Joints 1 and 2 and the other line passing Joints 3 and 4 is selected so that the compliant alignment axis lies exactly on the template-wafer interface. For fine orientation changes, the rigid body between Joints 2 and 3 rotates about an axis that is depicted by Point C in Figure 2.8 (the axis is normal to the paper). Since frictional contacts are undesirable for imprinting process due to particle contamination, all joints are made of flexure joints for the template orientation stage (Figure 2. 9). For a small motion range, such a flexure joint (notch) has been widely used.

A similar second flexure component is mounted orthogonally onto the first one so that the two orientation axes are orthogonal to each other and they lie on the interface. The flexure devices can be readily adapted to have open slots so that a curing UV light can pass through the template as required in lithographic applications. Parameters of each semi-circular notch have been determined based on the applied load and motion requirements. The spring coefficient of each semi-circular notch is desired to be low so that necessary orientation motions can be achieved with a minimum normal load between the template and wafer surfaces. Excessive loads may lead not only to undesirable large deformations but also to mechanical failure of either template or wafer. For the imprinting process, however, the template orientation stage should be able to support required imprinting load. The geometry of the semi-circular notch is designed so that when a $4N$ load is applied at $1cm$ off from the center, the stage rotates about 0.0005radian (Choi, 1999).

The verification of the analytical models of the template stages was performed using their FEM models. FEM analysis of these flexure structures showed that the template surface moved less than $5nm$ in the shearing direction for 0.00038radian tilting. It is believed that such small shearing motion can be accommodated by the compliance of the

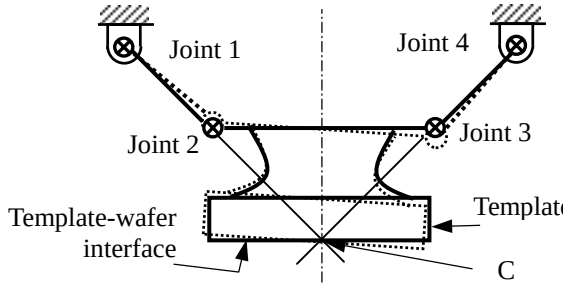

Figure 2.8 Four bar linkage composed of ideal joints and links: dotted one is the rotated configuration for a small angle

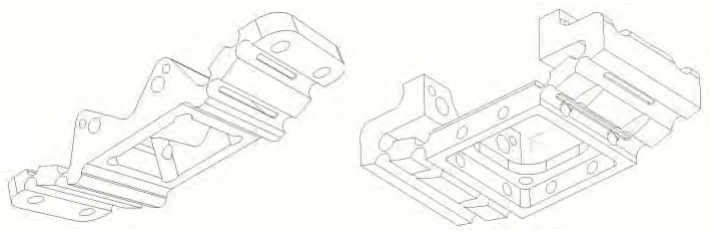

Figure 2.9 Two flexure template stages

patterning material.

3 DESIGN AND FABRICATION OF IMPRINT MACHINES

3.1 Single imprint machine with passive alignment stage

Figure 3.1 shows the SFIL single imprint prototype. To transfer an image, one first mounts a template in the template seat and places a silicon wafer on the orientation stage. The

template seat and orientation stage lie inside a press constructed of two horizontal plates and four 24*mm* diameter linear roller bearings. The roller bearings are preloaded to provide near-vertical motion between the template and the wafer. A linear actuator consisting of a brushless DC motor, a 1:160 harmonic drive, and a precision ground ball screw lowers the template until it rests directly above the silicon wafer. Once the template rests directly above the wafer, etch barrier polymer is dispensed and fills the gap between the template and the wafer via capillary action. After the etch barrier fills the gap between the template and wafer, the linear actuator presses the template onto the wafer. The wafer is mounted on a compliant orientation stage that flexes to allow the wafer to match the orientation of the template. After the template and wafer are in near-contact (assessed by force sensing), UV light illuminates the photo polymer. After the photo polymer is cross-linked, the linear actuator separates the template and wafer. The template and wafer may then be removed from the machine for inspection and further processing.

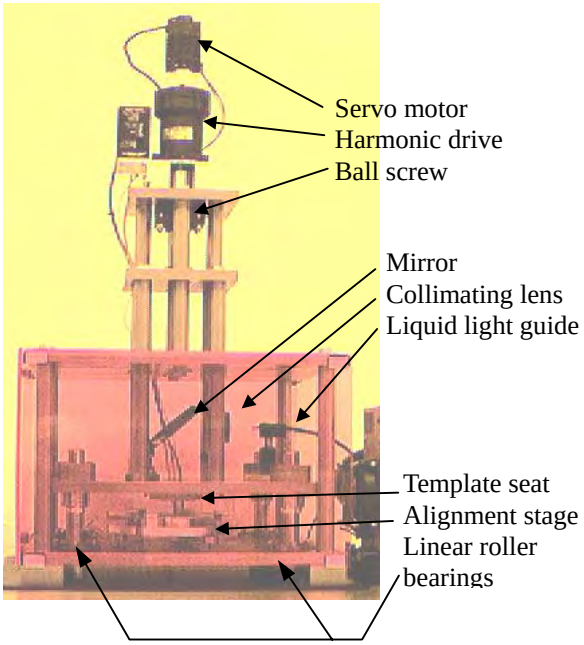

Figure 3.1 Single imprint machine

3.2 Multi imprint machine

Multi-imprint apparatus, shown in Figure 3.2, imprints repeated transferred images on 8" wafers similar to step and repeat semiconductor manufacturing. Each imprinting process is identical to that of the single imprint apparatus. A manual calibration stage, shown in Figure 3.3, is used to orient the template and wafer surface in parallel using interferometric techniques (Thompson, 1994). Here a visible monochromatic source was used to generate fringe pattern between the template lower surface and the wafer top surface. A manual inspection and calibration scheme that uses three differential micrometers allows the elimination of the fringe pattern. This implies that

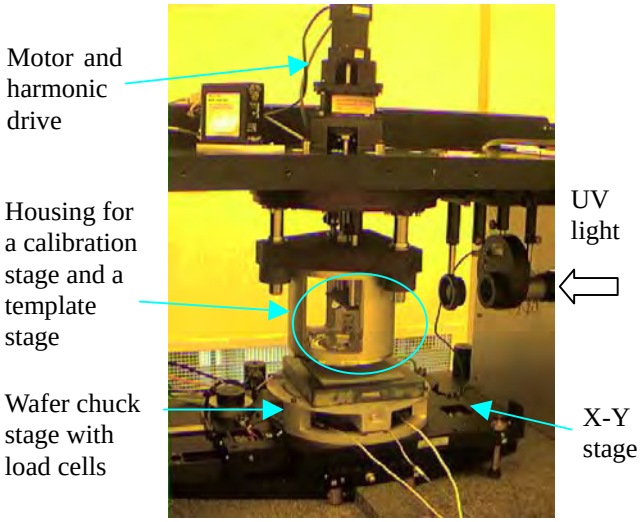

Figure 3.2 Multi-imprint apparatus

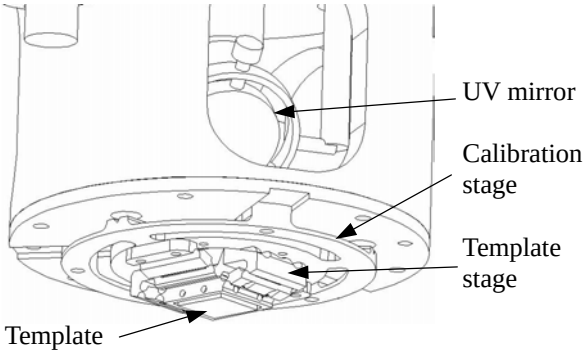

Figure 3.3 Assembly of calibration stage and template stage (circled area in Figure 3.2)

there is less than one fringe across the 1" by 1" template surfaces. This is equivalent to a variation of less than a quarter of the wavelength of the source across 1" by 1" template which results a wedging (Figure 1.4 (c)) of about 1μrad. The remaining misalignment between the template and wafer surface is compensated via the template stage that has remote compliance axes.

4 EXPERIMENTAL RESULTS

In this section, several imprint results are presented. High resolution flat templates were provided to this project by IBM in Burlington. Figures 4.1 (a) and (b) shows 60 *nm* features on template and wafer. It has been observed that SFIL process can duplicate not only such small features but also much smaller defects on the template due to stitching errors in the electron beam process. Hence, it is expected that the limit of feasible line width that SFIL can process is significantly smaller than 60 *nm*. However, 60*nm* line width is currently at the resolution limit of the template making process. Figure 4.1 (c) shows a

SEM image of 150*nm* features on the wafer surface. This view indicates that features have clearly defined side walls.

Figure 4.2 shows two 1" by 1" imprinted images where 12 blocks of features are imprinted. Figure 4.2 (a) contains several fringe patterns across its area, which indicates that the orientation between the template and wafer surface has not been properly compensated. Using the calibration stage, the template and wafer surfaces are oriented within one fringe across 1" by 1" (Figure 4.2 (b)). Figures 4.2 (b) and (c) show an active area with a wide spread fringe pattern and imprinted patterns respectively.

5 SUMMARY AND FUTURE WORK

Selectively compliant stages have been designed for single- and multi-imprint lithography machines. Successful

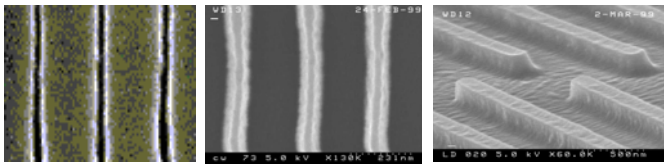

(a) (b) (c)

Figure 4.1 60*nm* features on template, (a), and wafer side, (b); (c) side walls on 150*nm* features

(a) (b) (c)

Figure 4.2 Imprint results: (a) Misalignment leads to a transferred image with several fringe patterns; (b) Less than one fringe pattern across 1" by 1" imprint area; (c) Enhanced pattern image of (b)

imprints have been demonstrated using imprint machines. Features that are less than 100*nm* have been successfully patterned. Current research focuses on investigating nano-resolution gap-sensing and design and control of active flexure stages.

ACKNOWLEDGMENTS

We gratefully acknowledge the financial support of DARPA (grant N66001-98-1-8914) and SRC (contract 96-LC-460)

REFERENCES

Badami, V.G., et al., 1996, "A Metrological Three-Axis Translator and its Application for Constant Force Profilometry", *Proceedings of ASPE 1996 Annual Meeting*, p. 391-395.

Choi, B. J. et al., 1999, "Design of Template Alignment Stages for Step & Flash Imprint Lithography", *Proc. of ASPE 1999 Annual Meeting*

Chou, S.Y., et al., 1996, "Nanoimprint lithography," *J. Vac. Sci. Technol*. B 1996, 14(6), 4129-33.

Colburn, M., et al., 1999, "Step and Flash Imprint Lithography: A Novel Approach to Imprint Lithography", *SPIE's 24th Annual International Symposium on Microlithography*, Santa Clara, CA.

Griffis, M., and Duffy, J., 1991, "Kinematic Control: A Novel Theory for Simultaneously Regulating Force and Displacement", *ASME Journal of Mechanical Design*, Vol. 113, pp.508-515.

Haisma, J., et al., 1996, "Template-assisted Nanolithography: A Process for Reliable Pattern Replication," *J. Vac. Sci. Technol*. B, 14(6), 4124-29.

Hunt, K. H., 1990, "Kinematic Geometry of Mechanisms", Oxford: Clarendon Press.

Johnson, S., 1999, "Selectively Compliant Orientation Stages for Imprint Lithography", MS thesis, The University of Texas at Austin.

Lee, K. M. and Shah, D., 1988, "Kinematic Analysis of a Three-Degrees-of Freedom In-Parallel Actuated Manipulator", *IEEE J. of Robotics and Automation*, vol. 4, no. 3, 354-360

Patterson, T., and Lipkin, H., 1993, "Structure of Robot Compliance," *ASME Journal of Mechanical Design*, Vol. 115, pp.576-580.

Roth, B., 1984, "Screws, Motors, and Wrenches That Cannot be Bought in Hardware Store," *Proceedings of the First International Symposium on Robotics Research*, MIT Press.

Stumbo, D. P., et al., 1991, *J. Vac. Sci, Technol*, B 9, 3597 (1991).

Smith, S., and Chetwynd, D.G., 1992, "Foundations of Ultraprecision Mechanism Design," Gordon and Breach Science Publishers, Philadelphia.

Thompson, L. F., et al., 1994, Introduction to Microlithography, 2nd Edition, ACS Professional Reference Book. American Chemical Society, Washington, DC.

Waldron, K. J., et al., 1989, "Kinematics of a Hybrid Series-Parallel Manipulation System," *ASME Journal of Dynamic Systems, Measurement, and Control*, vol. 111, pp. 211-221.

Waldron, K. J., 1993, Course Notes for ME 851 Kinematic Geometry of Mechanisms, The Ohio State University

Wang, D.; et al., 1997, "Nanometer scale patterning and pattern transfer on amorphous Si, crystalline Si, and SiO2 surface using self-assembled monomlayers," Appl. Phys. Lett., 70 (12).

Widden, T.K., et al., 1996, "Pattern Transfer to Silicon by Microcontact Printing and RIE," Nanotechnology, 7, 447-451.

Xia, Y. and Whitesides, G.M., 1998, "Soft Lithography," Angew. Chem. Int., 37, 550-575.

